4328 *Chem. Mater.* **2010,** *22,* 4328–4334
DOI:10.1021/cm1014459

CHEMISTRY OF MATERIALS
Article

A Multifaceted Cage Cluster, $[Co^{II}_6O_{12} \supset X]^-$ ($X = Cl^-$ or F^-): Halide Template Effect and Frustrated Magnetism

Qing Chen,[†] Ming-Hua Zeng,*[,†] Lian-Qiang Wei,[†] and Mohamedally Kurmoo*[,‡]

[†]*Key Laboratory of Synthetic and Natural Functional Molecule Chemistry of the Ministry of Education, Northwest University, Xi'an 710069, P. R. China, School of Chemistry & Chemical Engineering of Guangxi Normal University, Guilin 541004, P. R. China, and* [‡]*Laboratoire DECOMET, CNRS-UMR 7177, Université de Strasbourg, 4 rue Blaise Pascal, 67000 Strasbourg Cedex, France*

Received May 23, 2010. Revised Manuscript Received June 10, 2010

Two hexanuclear Co^{II} clusters, $NHEt_3[Co_6(phendc)_6 \supset X]\cdot MeOH\cdot 3H_2O$ ($X = Cl^-$ (**1**) or F^- (**2**)), were obtained accidently by the in situ formation of the coordinating ligand H_2phendc (1,10-phenanthroline-2,9-dicarboxylate) from the precursor ligand H_2phenox (1,10-phenanthroline-2,9-dicarbaldehyde dioxime). Halides among the reactants used become the template around which a highly symmetric cluster is generated which display spin-glass magnetic behavior as a consequence of the severe magnetic frustration due to geometrical arrangement of the moments. Different anion-template effects were demonstrated by ESI-MS studies. Interestingly, **1** exists in solution; in its solid state, a rare and unique single-crystal to single-crystal transformation is observed upon desolvation, which is accompanied by the departure of NEt_3. Both dc and ac magnetization data suggest the spin-glass behavior for **1** and its guest-free structure $H[Co_6(phendc)_6Cl]$ (**1′**) at different blocking temperatures of 5.3 and 7.8 K, respectively. The absence of this observation for **2** raises an interesting question regarding its origin and provides a remarkable example of fine-tuning of frustrated magnetic properties via host−guest interactions.

Introduction

Considerable efforts are being devoted to the field of coordination chemistry and in particular for metal−organic hybrids displaying several properties such as electrical, magnetic, optical, gas sorption, and catalysis.[1] The principal impetus being to design structures from building blocks, i.e. metals and ligands, having the structural, electronic and magnetic characteristics required for the desired properties in mind.[2] For example the use of open-shell metal ions and/or radical organic ligands for the design of molecular magnets.[1b] Consequently, it is a desire for scientists interested in several properties to attempt at controlling the crystal structures and the physical properties from the molecular structures of the starting building units.[3,4] However, while designing can be recognized in few cases, in general serendipity appears to have the upper hand.[5] Here, we report a case where two related multifaceted materials, $NHEt_3[Co_6(phendc)_6 \supset X]\cdot MeOH\cdot 3H_2O$ ($X = Cl^-$ (**1**) or F^- (**2**), H_2phendc = 1,10-phenanthroline-2,9-dicarboxylate), are obtained accidently; first by the in situ formation of the coordinating ligand, second, one element among the reactants used becomes the template around which a highly symmetric cluster is generated which display spin-glass magnetic behavior as a consequence of the severe magnetic frustration due to geometrical arrangement of the moments. These compounds provide good example where the size of the template can have a consequence on the magnetic behavior. Furthermore, **1** exists in solution and in its solid state where a rare and unique single-crystal to single-crystal transformation is observed upon desolvation, which is accompanied by the decomposition of the cation $(NHEt_3)^+$ to H^+ and the departure of NEt_3.

Experimental Section

Synthesis. All manipulations were performed under aerobic conditions, using chemicals and solvents as received unless otherwise stated. Ligand 1,10-phenanthroline-2,9-dicarbaldehyde dioxime (H_2phenox) was prepared as described and synthesized in an analogous manner.[6]

*Corresponding author. E-mail: zmh@mailbox.gxnu.edu.cn (M.-H.Z.); kurmoo@unistra.fr (M.K.).

(1) (a) Ma, S.; Zhou, H.-C. *Chem. Commun.* **2010**, *46*, 361–376. (b) Kurmoo, M. *Chem. Soc. Rev.* **2009**, *38*, 1353–1379. (c) Férey, G. *Chem. Soc. Rev.* **2008**, *37*, 191–214. (d) Lee, J.-Y.; Farha, O. K.; Roberts, J.; Scheidt, K. A.; Nguyen, S. T.; Hupp, J. T. *Chem. Soc. Rev.* **2009**, *38*, 1450–1459. (e) Wang, B.; Côté, A. P.; Furukawa, H.; O'Keeffe, M.; Yaghi., O. M. *Nature* **2008**, *453*, 207–211. (f) Sato., O. *Acc. Chem. Res.* **2003**, *36*, 692–700.

(2) (a) Miyasaka, H.; Yamashita, M. *Dalton Trans.* **2007**, 399–406. (b) Férey, G.; Serre, C. *Chem. Soc. Rev.* **2009**, *38*, 1380–1399. (c) O'Keeffe., M. *Chem. Soc. Rev.* **2009**, *38*, 1215–1217. (d) Roubeau, O.; Clérac, R. *Eur. J. Inorg. Chem.* **2008**, 4325–4342.

(3) (a) Batten, S. R.; Neville, S. M.; Turner, D. R. *Coordination Polymers Design, Analysis and Application*; The Royal Society of Chemistry: London, 2009. (b) Deng, H.; Doonan, C. J.; Furukawa, H.; Ferreira, R. B.; Towne, J.; Knobler, C. B.; Wang, B.; Yaghi, O. M. *Science* **2010**, *327*, 846–850.

(4) (a) Yaghi, O. M.; O'Keeffe, M.; Ockwig, N. W.; Chae, H. K.; Eddaoudi, M.; Kim, J. *Nature* **2003**, *423*, 705–714. (b) Janiak, C. *Dalton Trans.* **2003**, 2781–2804.

(5) (a) Saalfrank, R. W.; Maid, H.; Scheurer., A. *Angew. Chem., Int. Ed.* **2008**, *47*, 8794–8824. (b) Kong, X.-J.; Long, L.-S.; Zheng, Z.-P.; Huang, R.-B.; Zheng, L.-S. *Acc. Chem. Res.* **2009**, *43*, 201–209.

 Published on Web 06/30/2010

Table 1. Crystallographic Data

	1	2	1′
formula	$Co_6C_{91}H_{62}O_{28}N_{13}Cl$	$Co_6C_{91}H_{62}O_{28}N_{13}F$	$Co_6C_{84}H_{37}O_{24}N_{12}Cl$
fw	2174.6	2158.1	1987.3
cryst size (mm^3)	0.18 × 0.16 × 0.12	0.20 × 0.15 × 0.13	0.19 × 0.17 × 0.12
cryst syst	trigonal	trigonal	trigonal
space group	$R\bar{3}$	$R\bar{3}$	$R\bar{3}$
T (K)	173(2)	173(2)	353(2)
a (Å)	21.559(3)	21.530(2)	21.842(7)
c (Å)	16.642(5)	16.542(1)	14.502(9)
V (Å ^{3})	6698.8(2)	6640.5(7)	5991.6(5)
Z	3	3	3
D_c (g cm^{-3})	1.544	1.545	1.651
μ (mm^{-1})	1.205	1.187	1.339
no. of reflns [$I > 2\sigma(I)$]	2927	2604	2094
R_1 [$I > 2\sigma(I)$]	0.0435	0.0840	0.1217
wR_2 (all data)	0.1169	0.3110	0.3960
GOF	1.068	1.088	1.003
$\Delta\rho_{min/max}$ (e/Å^3)	−0.493/1.230	−0.596/1.455	−0.806/1.241

$R_1 = \sum||F_o| - |F_c||/\sum|F_o|$, $wR_2 = [\sum w(|F_o| - |F_c|)^2/\sum w|F_o|^2]^{1/2}$.

$NHEt_3[Co_6(phendc)_6Cl]\cdot MeOH\cdot 3H_2O$ (1). A mixture of $CoCl_2\cdot 6H_2O$ (1 mmol), H_2phenox (0.5 mmol), triethylamine (0.25 mL) and methanol (10 mL) were sealed in a 15-mL Teflon-lined, stainless-steel Parr bomb. The bomb was heated at 140 °C for 72 h. The red block crystals were obtained and picked out manually, washed with methanol and dried in air (yield 35% based on H_2phenox).

$NHEt_3[Co_6(phendc)_6F]\cdot MeOH\cdot 3H_2O$ (2). The procedure was similar to that of **1**, except that $CoF_2\cdot 2H_2O$ (1 mmol) was used instead of $CoCl_2\cdot 6H_2O$ (yield 33% based on H_2phenox).

$[Co_6(phendc)_6Cl]\cdot H$ (1′). **1′** was obtained by heating crystals of **1** from 25 to 130 °C at a heating rate of 10 °C/min, and kept at 130 °C for 0.25 h. They were then cooled down to room temperature. The completeness of the guest removal was monitored by TGA under N_2. All the crystals retained their primary well-defined external shapes after the heating process.

[Co(Hphenox)(phenoa)]·MeOH·$3H_2O$ (3). A mixture of $CoF_2\cdot 2H_2O$ (1 mmol), H_2phenox (0.5 mmol) and methanol (10 mL) was stirred at room temperature for 1 h, during which it turned red wine-color. The solvents were then removed. The reddish orange plate crystals formed were collected, washed with methanol, and dried under vacuum (yield 5% based on H_2phenox).

Materials and Physical Measurements. All reagents were commercially available and used without further purification. Infrared spectra were obtained from KBr pellets containing *ca.* 1% of the compounds on a PE Spectrum One FT-IR Spectrometer in the 400−4000 cm^{-1} region. Elemental analyses (C, H, N) were performed on a PE Series 2400 II CHNS Analyzer. Thermogravimetric analyses (TGA) were performed at a rate of 10 °C/min under N_2 using a Pyris Diamond TG/DTA thermogravimetric/differential thermal analyzer. Powder X-ray diffraction (PXRD) data were recorded on a Rigaku D/M-2200T automated diffractometer. Analytical pyrolysis was performed using a CDS Pyroprobe model 5200 pyrolyser with a platinum coil probe and gas chromatography−mass spectrometry using GC-2010 and GCMS-QP2010 Plus. AC and DC Magnetization measurements were performed on polycrystalline samples using a Quantum Design MPMS-XL7 SQUID. Data were corrected for the diamagnetic contribution calculated from Pascal constants and the sample container.

X-ray Crystallography. Diffraction data were collected on a Bruker Smart Apex CCD diffractometer with graphite-monochromated Mo-$K\alpha$ radiation (λ = 0.71073 Å). All intensity data were corrected for Lorentz and polarization effects, and empirical absorption corrections based on equivalent reflections were applied using SADABS.[7] The structures were solved by direct methods and refined by the full-matrix least-squares method on F^2 with SHELXTL program package.[8] All non-hydrogen atoms were refined with anisotropic displacement parameters. The hydrogen atoms of the ligand were generated geometrically, but no hydrogen atoms were added to the solvent molecules. The $HNEt_3^+$ cations could not be located because of their high degree of disorder. The CH_3OH molecules in **1** were treated using a disorder model consisting of two equivalent parts. The data of **1′** is less accurate because it is the high-temperature test at 353(2) K. Crystal data as well as details of data collection and refinements for **1**, **1′** and **2** are summarized in Table 1, summary of the geometrical data of exchange bridges is given in Table 2 and selected bond distances and bond angles are listed in Table S1 in the Supporting Information. CCDC reference numbers 765299−765302 for **1**, **1′**, **2** and **3**, respectively, which contain the supplementary crystallographic data for this paper. It can be obtained free of charge from the Cambridge Crystallographic Data Centre via http://www.ccdc.cam.ac.uk/data_request/cif.

Results and Discussion

Crystal Structure. Complex **1** was accidently obtained by the solvothermal reaction of H_2phenox (1,10-phenanthroline-2,9-dicarbaldehyde dioxime) and $CoCl_2\cdot 6H_2O$ in methanol under alkaline (triethylamine) conditions in the search for Co^{II} single molecule magnets. The X-ray structure of a red crystal of **1** consists of an anionic cage with *Ci*-symmetry, one encapsulated Cl^- ion sitting almost symmetrically in the center of the six Co^{II} forming a slightly distorted octahedron with Co···Co of 3.818(1)−3.825(1) Å (Figure 1). The cluster is bonded by six quadridentate chelating in situ generated $phendc^{2-}$ (Co−O 2.054(4)−2.400(3) Å, Co−N 2.142(5)−2.149(4) Å). Each Co^{II} adopts a rarely observed pentagonal-bipyramidal seven-coordination, CoO_2N_4Cl, with two oxygen

(6) (a) Chandler, C. J.; Deady, L. W.; Reiss., J. A. *J. Heterocyclic Chem.* **1981**, *18*, 599–601. (b) Angeloff, A.; Daran, J.-C.; Bernadou, J.; Meunier., B. *Eur. J. Inorg. Chem.* **2000**, 1985–1996.

(7) *SMART, version 5.0*; Bruker AXS: Madison, WI, 1998.*SAINTplus, version 6.0*; Bruker AXS: Madison, WI, 1999.*SHELXTL, version 6.1*; Bruker AXS: Madison, WI, 2001.

(8) *SHELXTL 6.10*; Bruker Analytical Instrumentation, Madison, WI, 2000.

Table 2. Summary of Geometrical Data of Exchange Bridges for 1, 2, and 1′ (in Å and deg)

1		2		1′		max deviation (%)
Co1a−O1−Co1	118.38(2)	Co1c−O1−Co1	118.80(3)	Co1e−O1−Co1	118.5(6)	0.35
Co1b−O3−Co1	117.95(2)	Co1d−O3−Co1	119.06(3)	Co1f−O3−Co1	119.540(1)	1.34
Co1···Co1a	3.818(1)	Co1···Co1c	3.784(3)	Co1···Co1e	3.783(4)	0.93
Co1···Co1b	3.825(1)	Co1···Co1d	3.771(3)	Co1···Co1f	3.853(4)	2.16
Co1−Cl	2.702(8)	Co1−F		Co1−Cl	2.699(3)	0.12
Co1a−Cl−Co1	89.89(2)	Co1c−F−Co1		Co1e−Cl−Co1	88.94(1)	1.10
Co1b−Cl−Co1	90.11(2)	Co1d−F−Co1		Co1f−Cl−Co1	91.06(1)	1.05

Symmetry codes: (a) $2-y, 1+x-y, z$; (b) $y, 1-x+y, -z$; (c) $-1+y, -x+y, -z$; (d):$1-y, 2+x-y, z$; (e) $1+x-y, 1+x, -z$; (f) $-1-x+y, 1-x, z$.

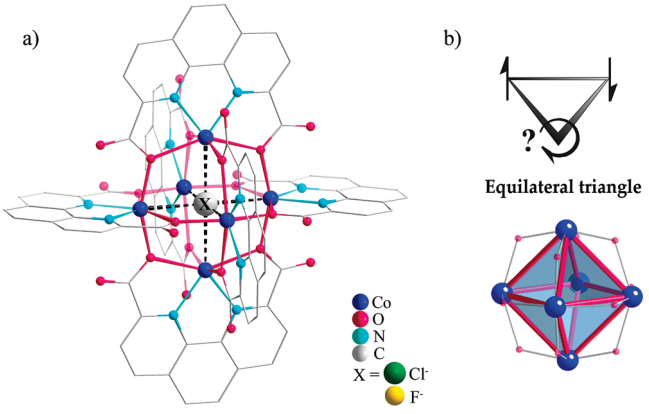

Figure 1. (a) Hexanuclear structure of $[Co_6(phendc)_6 \supset X]^-$ (X = Cl^- (**1**, **1′**) or F^- (**2**)); hydrogen atoms and uncoordinated molecules have been omitted for clarity; (b) spin frustration of antiferromagnetically coupled spins in an equilateral triangle presents in the cagelike model.

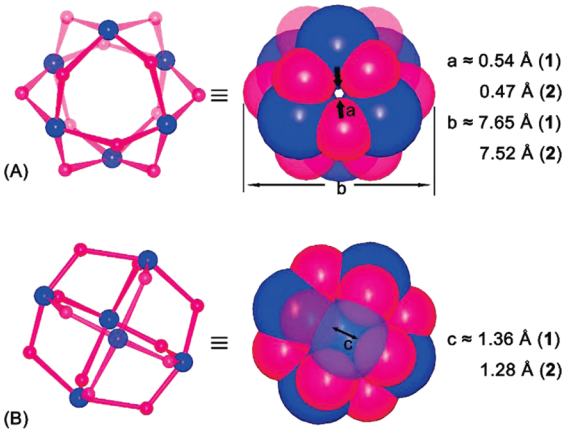

Figure 2. Dimensions of the cage and the cavity/window for **1** and **2**.

atoms in the axial positions at an angle of 157.02(1)° with the Co^{II} atoms. The central μ_6-Cl^- is weakly coordinated to the Co^{II} with an unusually long bond (Co−Cl 2.7023(1) Å, see Figure S1a in the Supporting Information), and make up the elongated equatorial O_2N_2Cl pentagon, which complete the distorted hepta-coordinated environment. One disordered $NHEt_3^+$ cation, three 1/3 occupied disordered methanol and three water molecules are located in the crystal lattice. The diameter of the $[Co_6O_{12}]$ core is ca. 7.65 Å, and the diameter of the cavity is ca. 1.36 Å, the cage is enclosed by eight edge-sharing Co_3O_3 windows, each one has the hexagonal entrance diameters of ca. 0.54 Å (van der Waals radii are taken into consideration, Figure 2). Interestingly, the template Cl^- is the charge carrier within a nominally neutral cluster and the cation resides outside the cluster. This is in contrast to the ferric wheel $[LiFe_6(OMe)_{12}(dbm)_6]$ and $[NaFe_6(OMe)_{12}$-$(pmdbm)_6]$, (Hdbm = 1,3-diphenyl-1,3-propanedione and Hpmdbm = 1,3-di(4-methoxyphenyl)-1,3-propanedione), where the cation is the template to charge balance the anionic cluster.[9]

The observation of the Cl^- anion in the center of the cage is an invitation to replace it with the other halides. It appears to be restricted to the size of the halide. Thus, when the same synthetic procedure was deliberately performed with $CoF_2 \cdot 2H_2O$ instead of $CoCl_2 \cdot 6H_2O$, **2** was isolated. The key feature of the crystal structure is identical to that of **1** with the consequence that F^- has short contacts with the surrounding Co^{II} ions (Co···F 2.671(3) Å, see Figure S1b in the Supporting Information) and the contraction of the core is due to the presence of the small F^- (Figure 2). Similar reactions starting with the bromide or iodide of cobalt were not successful. It is worth mentioning that in several examples of seven-coordinated Co^{II} complexes, most of which are mononuclear species except for examples of nitrate anions functioning as chelate ligands.[10] To the best of our knowledge, **1** is the first example with seven-coordinated Co^{II} complex comprising Cl^- atom in a high-nuclearity cluster.[11] High coordination numbers (higher than four) of Cl^- atoms centered in the cage serving as a weak ligand to transition metal ions were rarely reported (Figure 3); most are observed in copper and silver complexes,[12,13] and the μ_6 mode herein, is the first observed for Co^{II} complexes (Figure 4a).[14] Moreover, there are also several examples of metal polyhedra containing an encapsulated F^- ion.[15]

The in situ generation of the ligand is one of the key processes resulting in the formation of these clusters. The

(9) Cornia, A.; Affronte, M.; Jansen, A. G. M.; Abbati, G. L.; Gatteschi., D. *Angew. Chem., Int. Ed.* **1999**, *38*, 2264–2266.

(10) Masaoka, S.; Furukawa, S.; Chang, H.-C.; Mizutani, T.; Kitagawa, S. *Angew. Chem., Int. Ed.* **2001**, *40*, 3817–3819.

(11) *From the Molecular to the Nanoscale: Synthesis, Structure, and Properties*; Fujita, M., Powell, A., Creutz, C., Eds.; Elsevier: Oxford, 2004; Vol. *7*.

(12) (a) Toyota, A.; Yamaguchi, T.; Igashira-Kamiyama, A.; Kawamoto, T.; Konno., T. *Angew. Chem., Int. Ed.* **2005**, *44*, 1088–1092. (b) Liu, C.-W.; Hung, C.-M.; Haia, H.-C.; Liaw, B.-J.; Liou, L.-S.; Tsai, Y.-F.; Wang, J.-C. *Chem.Commun.* **2003**, 976–977.

(13) (a) Vilar, R. *Angew. Chem., Int. Ed.* **2003**, *42*, 1460–1477. (b) Bian, S.-D.; Wu, H.-B.; Wang, Q.-M. *Angew. Chem., Int. Ed.* **2009**, *48*, 5363–5365. (c) Bian, S.-D.; Jia, J.-H; Wang., Q.-M. *J. Am. Chem. Soc.* **2009**, *131*, 3422–3423.

(14) Allen, F. H.; Kennard, O. Chem. Des. Automat. News, **1993**, *8*, 31 (version 5.31, Feb 2010).

(15) Wang, Q.-M.; Guo, G.-C.; Mak, T. C. W. *Polyhedron* **2003**, *22*, 217–223.

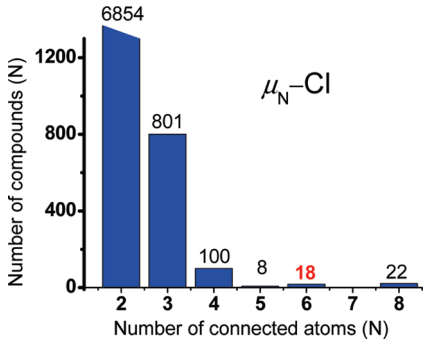

Figure 3. Statistical plot of the coordination numbers of Cl^- anion with transition metal ions.

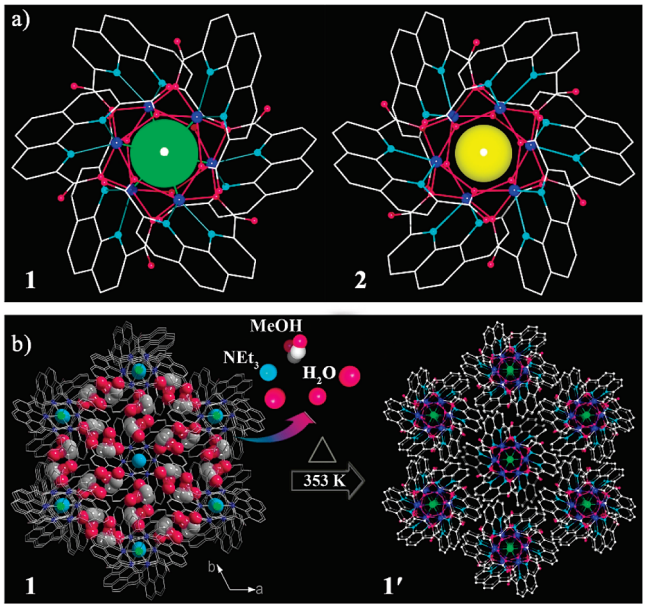

Figure 4. (a) Anion-centered assembly around octahedral Cl^- in **1** and weak coordinated F^- in **2** highlighted in space-filling modes; (b) SC-SC transformation from **1** to **1′**. Disordered NEt_3 are represented by fixed N atom and hydrogen atoms are omitted for clarity.

isolation of $[Co^{III}(Hphenox)(phenoa)]\cdot MeOH\cdot 3H_2O$ (**3**, phenoa = 1,10-phenanthroline-9-carbaldehyde oxime-2-carboxylate) suggests with some certainty that oxidation takes place stepwise for the ligand and also for the Co^{II}.[16] **3** consists of a monomeric Co^{III} with coordinating $phenoa^{2-}$ and $Hphenox^-$ ligands (see Figure S2 and Scheme S2 in the Supporting Information). Furthermore, the quadridentate ligand $phenoa^{2-}$ here, coordinated in the μ_3:η^2:η^1:η^1:η^2 fashion, has a fairly fixed distance between the two coordinating O-donors (4.54 ± 0.04 Å) of the carboxylate, which results in the rather long Co−O distance (2.38−2.40 Å). The enhanced coordination capability and rigid structure of $phendc^{2-}$ is not only helpful to construct high-nuclearity metal cluster but also give its complexes the high thermodynamic stability.

Things became more interesting when thermogravimetric analysis (TGA, see Figure S3 in the Supporting Information) of **1** was found to display a weight loss of 8.6% from 25 to 120 °C, corresponding to the loss of $3H_2O$,

(16) Chen, X.-M.; Tong, M.-L. *Acc. Chem. Res.* **2007**, *40*, 162–170.

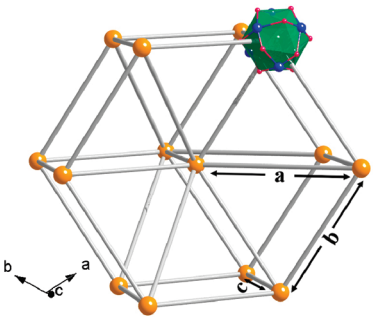

Center-Center distance of adjacent cluster (Å)

	1	2	1′
a	16.67	16.62	15.89
b	13.63	13.60	13.50
c	16.64	16.54	14.50

Figure 5. Illustrative representation of the link between Co_6 centers.

MeOH, and NEt_3 (8.5%) (Figure 4). The latter being confirmed using pyrolysis-gas chromatography−mass spectrometry (Py-GC/MS) method at 80 °C (see Figure S4 in the Supporting Information). This observation suggests the decomposition of the countercation. The resulting compound is stable to 400 °C. Through all the processes up to 400 °C, the framework of **1** retains its structural integrity based on the PXRD data (see Figure S5 in the Supporting Information). Microscopy shows that all the crystals retained their original well-defined external shapes and luster (photos in Figure 6a). Thus we were able to obtain, though irreversibly, the guest-free single crystals $H[Co_6(phendc)_6Cl]$ (**1′**). The single-crystal crystallographic study revealed that the hexanuclear core in **1′** resembles that of **1**, and the SC-SC transformation is accompanied by a structural contraction of 10.5% in cell volume from **1** to **1′**, because of shortening of the distances between neighboring clusters (Figure 5). This particular type of SC-SC is observed for the first time. SC-SC transformation is useful to develop new models for exploring the host−guest chemistry, which has been successfully demonstrated in many porous materials,[17,18] but only limited examples are known where clusters are involved, in which the changes of host environment play an important role in the construction of different molecular-based magnets.[19] Contrary to **1**, the same procedure by heating the crystals of **2** did not give the desired results, though the TGA is very similar, because of the poor crystallinity after transformation.

From the point of view of organic ligand design, it is an especially valid reason to use phenanthroline and its derivatives with their high tendency to form cage clusters because of their excellent chelating ability and large conjugated aromatic plane.[20] Following these considerations, we introduced the tetrapodant ligand 1,10-phenanthroline-2,9-dicarbaldehyde dioxime (H_2phenox), which resulted in the construction

(17) (a) Kawano, M.; Fujita, M. *Coord. Chem. Rev.* **2007**, *251*, 2592–2605. (b) Suh, M. P.; Cheon, Y. E. *Aust. J. Chem.* **2006**, *59*, 605–612. (c) Halder, G. J.; Kepert, C. J. *Aust. J. Chem.* **2006**, *59*, 597–604.

(18) (a) Zeng, M.-H.; Wang, Q.-X.; Tan, Y.-X.; Hu, S.; Zhao, H.-X.; Long, L.-S.; Kurmoo, M. *J. Am. Chem. Soc.* **2010**, *132*, 2561–2563. (b) Zeng, M.-H.; Hu, S.; Chen, Q.; Xie, G.; Shuai, Q.; Gao, S.-L.; Tang., L.-Y. *Inorg. Chem.* **2009**, *48*, 7070–7079. (c) Hu, S.; He, K.-H.; Zeng, M.-H.; Zou, H.-H.; Jiang, Y.-M. *Inorg. Chem.* **2008**, *47*, 5218–5224.

(19) (a) Cheng, X.-N.; Zhang, W.-X.; Chen., X.-M. *J. Am. Chem. Soc.* **2007**, *129*, 15738–15739. (b) Mishra, S.; Jeanneau, E.; Daniele., S.; Hubert-Pfalzgraf., L. G. *CrystEngComm.* **2008**, *10*, 814–816.

(20) Melton, D. L.; VanDerveer, D. G.; Hancock., R. D. *Inorg. Chem.* **2006**, *45*, 9306–9314.

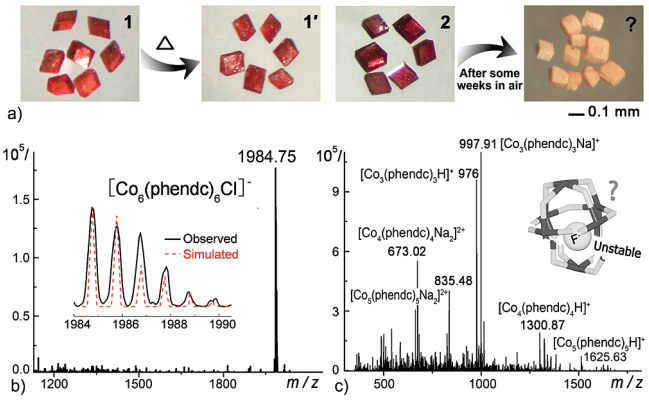

Figure 6. (a) Photos of crystals of **1**, **1′**, **2** and the light yellow substance coming from **2** in air. EIS-MS spectra of (b) **1** and (c) **2**.

of the two hexanuclear Co^{II} clusters $NHEt_3[Co_6(phendc)_6 \supset X]\cdot MeOH\cdot 3H_2O$ (X = Cl^- (**1**) or F^- (**2**)) and the guest-free structure $H[Co_6(phendc)_6 \supset Cl]$ (**1′**) obtained from **1** via SC-SC transformation. This series of halide-templated structures provide a good model system to test the magnetic properties modulated by the host−guest interactions in a frustrated system. Meanwhile, distinct stability of the clusters induced by halide-templated effects in solution and the unpredictable in situ generated H_2phenca ligand from H_2phenox under solvothermal condition are quite significant in deepening our understanding of the cluster assembly.

ESI-MS Studies. Characterization of the clusters in solution was performed by electrospray ionization mass spectroscopy (ESI-MS),[21] and it gives evidence of different halide-templated effects in the hexanuclear cages. For the acetonitrile solution of **1** (Figure 6b), the main peaks are observed at m/z 1984.75 as a result of **1** losing all solvent molecules and counterions to form $[Co_6(phendc)_6 \supset Cl]^-$, which agree well with the theoretical distributions. In contrast, we could not find the structure information of the integrated Co_6 cage when the same experiment was carried out for **2** (Figure 6c). Instead, the spectra display peaks associated with z = 1 or 2 charge states of $[Co_3(phendc)_3]$, $[Co_4(phendc)_4]$ and $[Co_5(phendc)_5]$ segments with H^+ and Na^+ counterions found at m/z of 976, 1300.87, 1625.63, 997.91, 673.02 and 835.48, respectively. The observed results corresponding to each peaks clearly matched with the assigned formulas as well as the simulated spectra (see Figure S6 in the Supporting Information). The unraveled species of cluster exist in solution phase showing the fragmentation of structure in **2**. The above observations may indicate that the Co_6 core preserves its structural integrity because of the stronger interaction of the incorporated Cl^- with the cobalt, whereas the unstable state of **2** is due to the weak interaction of F^-. It may also mean that if solvent can solubilize the fluoride, then **2** will be less stable, as found when the crystals are exposed to air (Figure 6a). ESI-MS studies not only helped us to identify and establish the integrity of the cluster but also to observe the different templating effect in stabilizing the cluster core. Hence, the

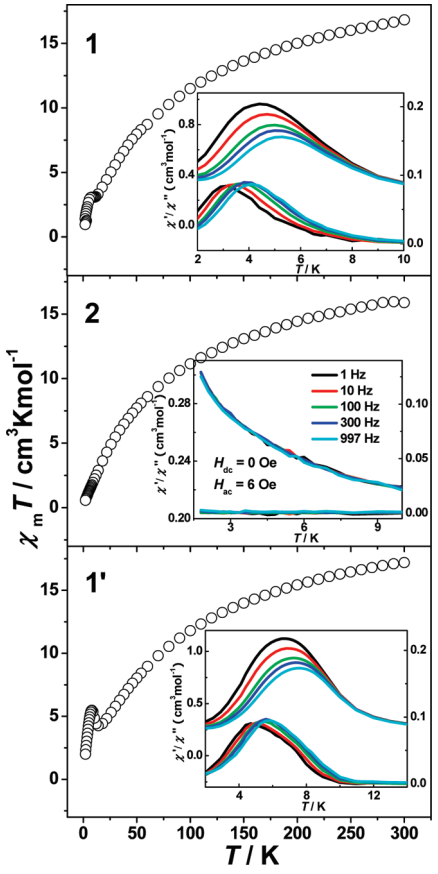

Figure 7. DC magnetic susceptibilities of **1**, **2** and **1′** recorded under a 1000 Oe field; inset, plots of in-phase (χ') and out-of-phase (χ'') ac susceptibilities.

present case offers a new example for the ESI-MS studies,[21,22] which has been successfully utilized to provide the information toward understanding the assembly of clusters in host−guest chemistry.

Magnetic Properties. The temperature-dependent magnetic susceptibilities of **1**, **2** and **1′** were measured on fresh polycrystalline samples with random orientations in dc-field of 1 kOe. The magnetic moments of the three samples are similar (Figure 7) at room temperature with $\chi_m T$ range of 15.9−17.2 $cm^3\ mol^{-1}\ K$, significantly larger than the spin-only value of six high-spin Co^{II} ions 11.3 $cm^3\ mol^{-1}\ K$. This is a common phenomenon for Co^{II} complex because of the orbital contribution.[23] Upon lowering the temperature, $\chi_m T$ of both **1** and **1′** first gradually decreases to a minimum value of 3.06 and 4.25 $cm^3\ K\ mol^{-1}$ at 10 and 14 K, where it goes to a shoulder with value of 3.07 and 5.46 $cm^3\ K\ mol^{-1}$ at 8.0 K, and finally decreases again on further cooling to 0.57 $cm^3\ mol^{-1}\ K$ at 2.0 K. There is no obvious anomaly in the dc susceptibility in **2**. The inverse magnetic susceptibility above 80 K obeys

(21) Miras, H. N.; Wilson, E. F.; Cronin, L. *Chem. Commun.* **2009**, 1297–1311.

(22) (a) Yan, J.; Long, D.-L.; Wilson, E. F.; Cronin, L. *Angew. Chem., Int. Ed.* **2009**, *48*, 4376–4380. (b) Newton, G. N.; Cooper, G. J. T.; Kögerler, P.; Long, D.-L.; Cronin., L. *J. Am. Chem. Soc.* **2008**, *130*, 790–791. (c) Li, B.-W.; Zhou, Y.-L.; Chen, Q.; Zeng, M.-H. *Polyhedron* **2010**, *29*, 148–153.

(23) (a) Zeng, M.-H.; Yao, M.-X.; Liang, H.; Zhang, W.-X.; Chen, X.-M. *Angew. Chem., Int. Ed.* **2007**, *46*, 1832–1835. (b) Chen, Q.; Zeng, M.-H.; Zhou, Y.-L.; Zou, H.-H.; Kurmoo, M. *Chem. Mater.* **2010**, *22*, 2114–2119.

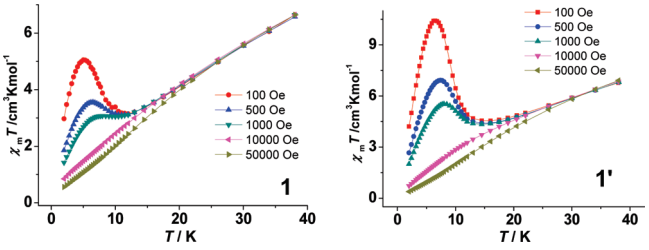

Figure 8. Plot of $\chi_m T$ vs T under different fields at low temperature for **1** and **1′**.

the Curie−Weiss law, giving the Curie constant C of 20.6 to 22.4 cm^3 mol^{-1}K and Weiss constant θ of −85 to −90 K (see Figure S7 in the Supporting Information). The effective moment per cobalt is 5.2 μ_B. The large negative θ values confirm the strong antiferromagnetic coupling between the intracluster Co^{II} ions. The dependence of χ_m vs T curves of **1** and **1′** at different fields is pronounced at low-temperature, the larger increase of χ_m values at a small field (Figure 8), which is an indication of the source of a resultant moment. Furthermore, they appear little perturbed by the presence of the solvents.

In search of our original aim, i.e., for single-molecule-magnetic behavior, we further investigate their magnetic properties at low temperature (2−30 K) using field-cooling magnetization (FCM) and zero-field-cooling magnetization (ZFCM) protocol for **1**, **2** and **1′** employing 20 Oe applied field (see Figure S8 in the Supporting Information). The FCM and ZFCM data show bifurcation at 6.3 and 8.8 K for **1** and **1′**, respectively. In addition, we performed a series of ac-susceptibilities measurements at different frequencies using an oscillating field of 6 Oe and a zero dc-field. From the temperature dependence of ac magnetic susceptibilities (Figure 7 inset), **1** and **1′** clearly show a nonzero out-of-phase signal χ'' with a peak at ca. 4 and 5.7 K, respectively, accompanied by a broad one for χ'; both having a small frequency-dependent behavior. The shift is to the high temperature with increasing frequency. The correspondence between the bifurcation in ZFC/FC and the peaks in the ac-susceptibilities is to be noted. Interestingly, none of these were observed for **2** within the experimentally available temperatures. However, the broad features are uncharacteristic of long-range magnetic ordering and the small frequency dependence is likewise uncharacteristic of SMM.[23,24] However, both can be related to superparamagnetism of small particles or spin-glass behavior. The shift of the peak temperature (T_p) of χ' was measured by a parameter $\phi = \Delta T_p/[T_p \Delta(\log\omega)] = 0.052$ for **1** and 0.041 for **1′**, corresponding to a canonical spin glass.[25] The relaxation time was obtained from the Arrhenius law $\tau = \tau_0 \exp(-\Delta/k_B T)$; the best set of parameters are $\tau_0 = 1.29 \times 10^{-13}$ s and $\Delta/k_B = 86$ K for **1** and $\tau_0 = 3.5 \times 10^{-17}$ s and $\Delta/k_B = 170$ K for **1′**.

The field-dependence of the magnetization was also studied at very low temperatures (see Figure S9 in the Supporting Information). Magnetization curves of **1** and **1′** at 2 K are similar, exhibiting an increase of the magnetization in the low-field region, and then increase slowly and linearly with the field. A pronounced slope of the magnetization curve is observed for **2** at 2 K. The non-Brillouin and linear dependence of the magnetization attaining values of 1.9 $N\beta$ (**1**), 1.9 $N\beta$ (**1′**) and 2.5 $N\beta$ (**2**) per Co_6 unit at 7 T, which are below the expected saturation value for spin-only Co^{II} species, are characteristics of the presence of antiferromagnetic interactions. A very small hysteresis exists in the low field at 2 K for **1** with the coercive field H_c = 190 Oe. The shape and temperature dependence changes of magnetization curve for **1′** is similar to **1** with a slightly wider H_c = 350 Oe. However, no hysteresis loop is observed for **2**.

Both dc and ac magnetization data suggest the spin glass behavior for **1** and **1′** with slightly different blocking temperatures and none for **2**. This observation raises an interesting question regarding its origin. There is one way of looking at the problem. First, one may consider that the long distances between Co and the halide provide very weak exchange and the dominating exchange is through the μ-oxo bridges and this is antiferromagnetic (Table 2). Consequently, the near equilateral triangular face of the octahedron results in geometrical spin frustration (Figure 1b), thus the high value (above 20) for θ/T_B, where T_B is the blocking temperature of the spin-glass. This is consistent with the observation that **1** and **1′** behave in a similar way. It is also understandable that the blocking temperature is slightly higher for the latter which may be associated with the slight contraction of the cluster (Table 2, Figure 5). It can be noted that the intercluster interactions is extremely weak or nonexistent. However, using the above argument one expects a similar behavior at a higher T_B for **2** and this is not the case. To explain the latter, we need to assume that the exchange through the halide cannot be neglected at low temperatures. If this is included we then have both antiferromagnetic exchange Co−X−Co of 180° and ferromagnetic for 90° as expected by the Goodenough-Kanamori rule in addition to the exchange within the face. The presence of both types of interaction introduces additional frustration of the moments within each cluster. However, the difference in bond distances and in exchange values due to the different electronic density of the halide may be responsible for the higher T_B in the case of chloride. The present results suggest that we should add the octahedron in the list of magnetic frustrated geometries which include the triangle (trimer and Kagomé network) and the tetrahedron (tetramer and pyrochlore framework).[26−28] For

(24) Gatteschi, D.; Sessoli, R.; Villain, J. *Molecular Nanomagnets*; Oxford University Press: Oxford, U. K., 2006.
(25) ϕ = 0.01 is a typical value for a spin glass. For details, see Mydosh, J. A. *Spin Glasses: An Experimental Introduction*; Taylor & Francis: London, 1993.
(26) Greedan., J. E. *J. Mater. Chem.* **2001**, *11*, 37–53.
(27) (a) Daniel, C.; Hartl, H. *J. Am. Chem. Soc.* **2009**, *131*, 5101–5114. (b) Han, Y.; Shokef, Y.; Alsayed, A. M.; Yunker, P.; Lubensky, T. C.; Yodh, A, G. *Nature* **2008**, *456*, 898–903. (c) Machida, Y.; Nakatsuji, S.; Onoda, S.; Tayama, T.; Sakakibara, T. *Nature* **2010**, *463*, 210–213. (d) Mengotti, E.; Heyderman, L. J.; Fraile Rodríguez, A.; Bisig, A.; Le Guyader, L.; Nolting, F.; Braun, H. B. *Phys. Rev. B* **2008**, *78*, 144402.
(28) (a) Zheng, Y.-Z.; Tong, M.-L.; Xue, W.; Zhang, W.-X.; Chen, X.-M.; Grandjean, F.; Long, G. J. *Angew. Chem., Int. Ed.* **2007**, *46*, 6076–6080. (b) Wang, X.-Y.; Wang, L.; Wang, Z.-M.; Gao, S. *J. Am. Chem. Soc.* **2006**, *128*, 674–675. (c) Zhang, W.-X.; Xue, W.; Lin, J.-B.; Zheng, Y.-Z.; Chen, X.-M. *CrystEngComm.* **2008**, *10*, 1770–1776. (d) Zeng, M.-H.; Feng, X.-L.; Zhang, W.-X.; Chen., X.-M. *Dalton Trans.* **2006**, 5294–5303.

example, the control of the exchange coupling within the octahedral clusters [$GdNi_6$] and [$LaNi_6$] through the central rare earth atom has been achieved,[29] while fine-tuning of the magnetic anisotropy has been demonstrated for the $Fe_6(OMe)_{12}^-$ wheels through the different alkali metals (Li^+ or Na^+).[9]

Conclusion

This series of hexanuclear Co^{II} clusters provides a rare set of characteristics including in situ solvothermal generation of ligand, templated crystallization, high symmetry, irreversible single-crystal to single-crystal transformation upon desolvation accompanied by the unique decomposition of the cation, existence in solution, and geometrical spin frustration leading to a spin-glass ground state where the blocking temperature depends on the template. To the best of our knowledge, there is no precedence to this range of characters for one complex.

(29) Yasuhiko, Y.; Guillem, A.; Satoshi, I.; Joan, R.; Zvyagin, S. A.; Krzystek., J. *Angew. Chem., Int. Ed.* **2005**, *44*, 1997–2001.

Acknowledgment. This work was supported by NSFC (20871034), NSFGX (00832001Z), Program for New Century Excellent Talents in University of the Ministry of Education China (NCET-07-217), Project of Ten, Hundred, Thousand Distinguished Talents in New Century of Guangxi (2006201), Ying Tung Education Foundation (111014), and the Université de Strasbourg and CNRS (France).

Supporting Information Available: Crystallographic data (CIF); XRD and TG measure, Py-GC/MS measures of **1**, plots of χ^{-1} vs T, the fit of Curie−Weiss law at some different temperatures ranges and M vs H, and EIS-MS spectra and its simulated plots of **2** (PDF). This material is available free of charge via the Internet at http://pubs.acs.org.